The Journal of Chemical Physics

# A hydrated ion model of $[UO_2]^{2+}$ in water: Structure, dynamics, and spectroscopy from classical molecular dynamics

Cite as: J. Chem. Phys. **145**, 224502 (2016); https://doi.org/10.1063/1.4971432
Submitted: 22 September 2016 . Accepted: 21 November 2016 . Published Online: 15 December 2016

Sergio Pérez-Conesa, Francisco Torrico, José M. Martínez, Rafael R. Pappalardo, and Enrique Sánchez Marcos



# A hydrated ion model of $[UO_2]^{2+}$ in water: Structure, dynamics, and spectroscopy from classical molecular dynamics

Sergio Pérez-Conesa, Francisco Torrico, José M. Martínez, Rafael R. Pappalardo, and Enrique Sánchez Marcos[a)]
*Departamento de Química Física, Universidad de Seville, 41012 Seville, Spain*

(Received 22 September 2016; accepted 21 November 2016; published online 15 December 2016)

A new *ab initio* interaction potential based on the hydrated ion concept has been developed to obtain the structure, energetics, and dynamics of the hydration of uranyl in aqueous solution. It is the first force field that explicitly parameterizes the interaction of the uranyl hydrate with bulk water molecules to accurately define the second-shell behavior. The $[UO_2(H_2O)_5]^{2+}$ presents a first hydration shell U–O average distance of 2.46 Å and a second hydration shell peak at 4.61 Å corresponding to 22 molecules using a coordination number definition based on a multisite solute cavity. The second shell solvent molecules have longer mean residence times than those corresponding to the divalent monatomic cations. The axial regions are relatively de-populated, lacking direct hydrogen bonding to apical oxygens. Angle-solved radial distribution functions as well as the spatial distribution functions show a strong anisotropy in the ion hydration. The $[UO_2(H_2O)_5]^{2+}$ solvent structure may be regarded as a combination of a conventional second hydration shell in the equatorial and bridge regions, and a clathrate-like low density region in the axial region. Translational diffusion coefficient, hydration enthalpy, power spectra of the main vibrational modes, and the EXAFS spectrum simulated from molecular dynamics trajectories agree fairly well with the experiment. *Published by AIP Publishing.* [http://dx.doi.org/10.1063/1.4971432]

## I. INTRODUCTION

Actinide solution chemistry is an important challenge for many fields in science. The development of nuclear technology, its waste reprocessing, and its environmental impact involve a wide set of areas in physics, chemistry, biology, geology, and engineering.[1] Spent nuclear fuel contains many radioactive cations in the form of hydrated actinyls, $[AnO_2(H_2O)_m]^{q+}$,[2–8] that become the normal way these species are selectively separated and stored.[9] The mobility of uranyl and other actinyls determines their speciation in natural aqueous systems, in contaminated water, in storage tanks, and their potential escape from permanent geological repositories. Due to the long lifetime of the radioactivity and the large number of environments, the problem exceeds laboratory scale. Then, the generation of appropriate inexpensive and realistic models of the phenomena becomes a challenge. Computer simulations of actinyls in solution or in other environments are a step forward in the theoretical description of radioactive materials.

With the development of accurate heavy-element quantum-mechanical (QM) techniques[10–14] in the last decade, an increasing number of theoretical works have supplied a first-principles description of the bonding properties of these species.[15–17] Since the early studies, solvent effects were recognized as an important factor to be considered. They were accounted either by a discrete model of one or two solvation shells,[18–22] or by the inclusion of the hydrated ion within a dielectric continuum,[23–29] as had previously been proposed for other metal cation hydrations.[30,31]

The powerful QM approach must be completed with a statistical mechanical picture of the dynamic hydration phenomenon. Even though *ab initio* molecular dynamics is ideal to this aim, in practice its computational cost limits the system size and simulation times. Fortunately, classical statistical simulations sample the ensemble in an effective way allowing to reach the necessary system sizes and simulation time scales. But this is only reliable if the interaction potentials describe properly the potential energy surface and no chemical change takes place in the system. Therefore, robust potential generation must be based on accurate experimental data and/or QM results. Due to the experimental difficulties associated with radioactive materials, information for many cations in condensed phase is scarce,[32] hindering empirical potential development. *Ab initio* data can be obtained and force fields can be systematically improved by adding ion-water structures to the model potential energy surface and by increasing the level of theory.

Guilbaud and Wipff[33] pioneered in $[UO_2]^{2+}$ force field development in the 1990's. Their model is empirical and was fitted to reproduce the hydration free energy of the molecular cation. Kerisit and Liu updated the model changing the partial charges in order to reproduce a more recent value of hydration free energy.[34]

*Ab initio* force fields have also been published. Hagberg *et al.*[35] used the NEMO approach[36] to generate intermolecular potentials from multireference QM computations and carried out molecular dynamics (MD) simulations. In this work the importance of introducing charge transfer terms to describe

[a)]Electronic mail: sanchez@us.es

the hydrate of a doubly charged ion in solution, such as uranyl, was shown. Maginn *et al.*[37,38] considered the importance of polarization and other many-body effects in the binding of water molecules to the cation. They developed another first-principles force field for uranyl by parameterizing the interaction energies of the cation in the presence of four hydration water molecules.

Bühl *et al.*[39] obtained interesting results associated with the dissociation process of one water molecule from the uranyl hydrate in solution by Car-Parrinello MD,[40] showing the predominance of the penta-coordination of uranyl with respect to the tetra-coordination. Nichols *et al.*[41] ran a similar simulation, using an ensemble of snapshots to satisfactorily predict the EXAFS spectrum of uranyl. Frick *et al.*[42] used a QM/ MM Hartree-Fock-Mulliken charge Hamiltonian to carry out an MD simulation in which they studied the angularly resolved radial distribution functions.

All these theoretical studies along with experimental evidence[3,43] establish a first hydration shell of five water molecules with an average $D_{5h}$ symmetry and an experimental residence time longer than 1 $\mu$s.[44,45] Classical force fields have always underestimated this exchange rate by several orders of magnitude (unless particular constraints are imposed[46]) and typically display water exchange. The exchange should not happen since it has an experimental period longer than the simulation time.

Most *ab initio* ion force fields are pairwise and based on the interaction of a dimer, the ion, and a single water molecule. One of the problems of the dimer description is an overestimation of the interaction as a consequence of the electrical polarization of a single solvent molecule by the cation. Maginn *et al.* showed that effective pair-wise interaction potentials are necessary to study $[UO_2]^{2+}$ in aqueous solution.[37] Also, for highly charged cations, the true dissociation limit of the aggregate $[M(H_2O)]^{m+}$ usually is the charge transfer state $M^{(m-1)+} + H_2O^+$ instead of the required $M^{m+} + H_2O$.[47] In addition, the electronic state of *d* and *f* series metals with partially filled orbitals can be altered during the computation of the scans needed to collect QM interaction energies for the intermolecular potential fit, since the water-ion distance has to be changed significantly.

The general and cheapest strategy to model ion-water interactions in classical MD is to represent the ion as a charged particle with a Lennard-Jones potential to incorporate van der Waals interactions (a "charged soft sphere" model). This model has the advantage of being very simple and straightforward to transfer to other systems using Lorentz-Berthelot combination rules, but has limited accuracy. For instance, it neglects charge transfer and the polarization effects on the first-shell water molecules. In addition, it treats the interaction of the first-shell water molecule with the bulk solvent as equivalent to the interactions inside the bulk, neglecting the polarization that first-shell molecules are subjected to.

The model was developed by Maginn *et al.*[37] and was included in their force field fitting QM structures containing $[UO_2]^{2+}$ and several solvation water molecules. In this way they depart from the dimer approach and for transferability use the "charged soft sphere" representation. Even though the first-shell exchange rates are several orders of magnitude high with respect to experiment,[46] the model overall reproduces experimental data and gives insight into the nature of the solution.

We have taken a new step forward modelling $[UO_2]^{2+}$ as a hydrated ion which parameterizes the *ab initio* interaction of bulk water with the pentahydrate. Several years ago, our group proposed[48–51] a specific strategy to build first-principles intermolecular potentials of highly charged metal cations in water on the basis of the old electrochemistry concept of the *hydrated ion*. It states that most metal and highly charged monatomic cations ($M^{n+}$) in aqueous solutions are better represented by their hydrated ion, $[M(H_2O)_m]^{n+}$.[44] The implementation of the hydrated ion concept reasonably describes structural, dynamical, energetic, and spectroscopical properties of aqueous solutions containing metal cations forming well defined *aquaions* in water.[49,51–53] A second step was achieved when square-planar aquaions, such as $[Pd(H_2O)_4]^{2+}$ and $[Pt(H_2O)_4]^{2+}$, were studied.[54,55] We observed that the region above and below the water molecule plane differs from the conventional first or second-shell hydration behavior. The *meso-shell* concept was proposed to describe this region.[54] For the hydrated actinyls, there are formal topological similarities with the square-planar aquaions, placing actinyl oxygens above and below the plane. There is asymmetry around the central cation, since the axial regions are quite different from the equatorial region that accommodates the first hydration shell. The aim of this work is to provide a global image of $[UO_2(H_2O)_5]^{2+}$ hydration using MD implementation of an *ab initio* force field based on the hydrated ion model.

## II. METHODS

### A. Hydrated ion model potential for uranyl

The implementation of the hydrated ion concept assumes there are two different types of water molecules in solution.[48,49,56] Those of the first-shell bearing strong polarization effects and partial charge transfer from their direct interaction with the metal cation, and the rest of the water molecules belonging to the bulk solvent. Therefore, two different ion-water interaction potentials must be defined: IW1, (ion-water of the 1st shell) dealing with the ion-first-shell water molecules, and HIW, (hydrated ion-water) which describes the interaction of the hydrated ion with the bulk water molecules. Figure 1 displays a schematic representation of the regions where the different interaction potentials apply. The benefit of a refined discrimination among the first-shell and bulk water molecules has a price to pay, the water molecules of the first shell cannot exchange with the bulk water molecules. They are assumed to remain in the first shell, then this model precludes the analysis of the water exchange. Therefore, the validity of this hydrated ion model is constraint to the description of stable metal aquaions whose lifetimes are greater than simulation time. Additional to the ion-water potentials, a water model is chosen to describe the water-water interactions in the bulk. In the first shell these water-water interactions are given by the QM partial charges and the bulk water van der Waals interaction. Details of the previous development can be found elsewhere.[50,51,56] In the case of the uranyl, an intramolecular potential for the cation is necessary, hereafter called IMC (Intra Molecular Cation), to make $[UO_2]^{2+}$ flexible.

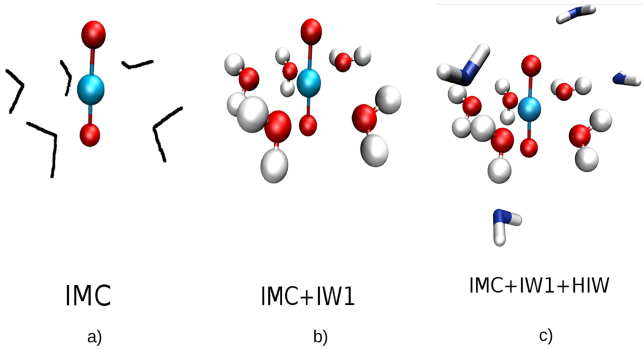


FIG. 1. Schematic representation of the different potentials describing uranyl in water. The intramolecular cation potential (IMC, (a)) corresponds to the interaction within the molecular cation. The ion-1st-shell water potential (IW1, (b)) describes the interaction of the first shell and the uranyl. The hydrated ion water potential (HIW, (c)) defines the interaction of bulk water molecules and $[UO_2(H_2O)_5]^{2+}$.

QM calculations at the B3LYP level[57,58] were used to compute the interaction energies, $E_{int}$, needed to build all the interaction potentials as well as the geometry optimization for the reference structure. The relativistic effective core pseudopotentials (RECP) of the Stuttgart group were used for the uranium atom with the recommended basis sets[59] [12s11p10d8f2g]/[8s7p6d4f2g]. The aug-cc-pVDZ basis set was employed for the rest of the atoms.[60] Several authors have shown that this hybrid functional method gives for uranyl reliable results at low computational cost.[17,21,27] All these calculations have been performed with the Gaussian09 program.[61]

The basic unit for the development of the different potentials is the pentahydrated uranyl(VI) ion, $[UO_2(H_2O)_5]^{2+}$, since it has been proposed to be the most stable aquaion[6,39,62,63] even though an equilibrium with the tetrahydrate has also been suggested.[62] The reference structure is obtained by QM geometry optimization enforcing $D_{5h}$ symmetry. The effective partial charges on the different atoms are obtained by the Merz-Kollman method[64,65] using the polarizable continuum model[66,67] to represent the bulk solvent polarization in the DFT calculation. Batsanov's radii for U were used to compute the charges.[68] The partial charges used are given in Table S1 of the supplementary material.

The intermolecular potential IW1 ($E_{IW1}$) describes the $UO_2$–$(H_2O)_I$. The QM energy information to fit this potential is obtained from a set of 150 structures taken from the displacement of U–($H_2O$) distance for one of the first-shell water molecules in the range 2.10-3.10 Å, and deformations of the $[UO_2]^{2+}$ following the stretching normal vibrational modes (symmetric and asymmetric) for U–$O_{yl}$ bond-lengths of 1.55-1.85 Å, and the bending normal mode in the range 180°–150°. A schematic representation of the deformations is given in Figure S1 of the supplementary material. The QM interaction energy for a given structure $i$ is obtained from the following expression:

$$E^i_{int} = E^i_{[UO_2(H_2O)_5]^{2+}} - E^i_{UO_2^{2+}} - 5E_{(H_2O)_I}. \quad (1)$$

These interaction energies, $E^i_{int}$, can be decomposed into two terms, one of them corresponding to the actinyl-water molecules interaction, i.e., $E_{IW1}$, and the other to the water molecules among them. Then Equation (2) associates the QM interaction energy and the classical intermolecular potentials,

$$E_{int} = E_{IW1} + E_{(H_2O)_I-(H_2O)_I}. \quad (2)$$

$E_{(H_2O)_I-(H_2O)_I}$ is computed using for the electrostatic part the Merz-Kollman charges of the hydrated ion (Table S1 in the supplementary material) and the short-range term of the TIP4P water model. The *ab initio* interaction energy of actinyl-first-shell water molecules is then fitted to the following site-site pair potential functional form:

$$E_{IW1} = \sum_i^{\substack{UO_2\\sites}} \frac{C^{iO}_4}{r^4_{iO}} + \frac{C^{iO}_6}{r^6_{iO}} + \frac{C^{iO}_8}{r^8_{iO}} + \frac{C^{iO}_{12}}{r^{12}_{iO}} + \sum_i^{\substack{UO_2\\sites}} \sum_j^{\substack{Water\\sites}} \frac{q_i q_j}{r_{ij}}. \quad (3)$$

Charges and coefficients of the fitting and root mean square error (RMSE) are given in Table S2 of the supplementary material.

The flexibility of uranyl is described by the IMC interaction potential, which models the actinyl as three particles, the two $O_{yl}$ and the uranium cation, U(VI). The interaction energy among these three particles is computed as the formation energy of the molecular cation

$$U^{6+} + 2\,O^{2-} \longrightarrow UO2^{2+}.$$

The QM energy for the actinyl cation $E^i_{UO_2^{2+}}$ in one of the distorted structures used to compute $E^i_{int}$ for the IW1 potential could be decomposed as a sum of the absolute energy of the separated atoms and the interaction energy among them,

$$E^i_{UO_2^{2+}} = E_{U^{6+}} + 2E_{O^{2-}} + E^i_{int}(UO_2^{2+}). \quad (4)$$

In this way the total interaction energy including the flexibility of the actinyl cation can be written by the following expression:

$$E^{tot}_{int} = E_{[UO_2(H_2O)_5]^{2+}} - E_{U^{6+}} - 2E_{O^{2-}} - 5E_{(H_2O)_I}, \quad (5)$$

where $(H_2O)_I$ denotes a water molecule with the geometry of the first hydration shell. This total interaction energy may be now split into three intramolecular components,

$$\begin{aligned} E^{tot}_{int} &= E_{int} + E^i_{int}(UO_2^{2+}) \\ &= E_{IMC} + E_{IW1} + E_{(H_2O)_I-(H_2O)_I}. \end{aligned} \quad (6)$$

From this relationship, we derive the intramolecular interaction energy for the molecular cation in a given geometry,

$$E_{IMC} = E^{tot}_{int} - (E_{IW1} + E_{(H_2O)_I-(H_2O)_I}). \quad (7)$$

In this way, the intramolecular interaction inside the uranyl cation is associated with the change in the formation energy of the actinyl from their corresponding monatomic charged ions. This way of defining $E_{IMC}$ guarantees the coupling among the different potentials. Making use of the hydrated ion concept, the flexibility of $UO_2^{2+}$ is computed inside the hydrated ion, extracting the changes in the relative energy of the actinyl unit in the presence of the first-shell water molecules. The different deformation geometries lead to a set of values for $E_{IMC}$ to be fitted to the following functional form:

$$E_{\mathrm{IMC}} = \sum_{i}^{\substack{\mathrm{O_{yl}}\\ \mathrm{sites}}} \left( \frac{C_4^{\mathrm{AnO_{yl}}}}{r_{\mathrm{AnO_{yl}}}^4} + \frac{C_6^{\mathrm{AnO_{yl}}}}{r_{\mathrm{AnO_{yl}}}^6} + \frac{C_8^{\mathrm{AnO_{yl}}}}{r_{\mathrm{AnO_{yl}}}^8} + \frac{C_{12}^{\mathrm{AnO_{yl}}}}{r_{\mathrm{AnO_{yl}}}^{12}} \right) + \sum_{i}^{\substack{\mathrm{O_{yl}}\\ \mathrm{sites}}} \frac{q_{\mathrm{An}} q_{\mathrm{O_{yl,i}}}}{r_{\mathrm{AnO_{yl,i}}}}. \quad (8)$$

Coefficients of the fitting and RMSE are given in Table S3 of the supplementary material.

To fulfill the description of the system, the interaction between the bulk water molecules and the hydrated actinyl must be considered, i.e., $[UO_2(H_2O)_5]^{2+}$–$H_2O$, the HIW potential. No other force field for $[UO_2]^{2+}$ in the literature has given a specific first shell-second shell water interaction potential, the other strategies approximate this interaction by the bulk-bulk water interaction. A probe water molecule is placed at different distances and orientations with respect to the actinyl aquaion as shown in Figure 2. Around 1000 single QM points have been computed to get the interaction of a bulk water molecule with the aquaion

$$E_{\mathrm{int}} = E_{[UO_2(H_2O)_5]^{2+}\text{–}H_2O} - E_{[UO_2(H_2O)_5]^{2+}} - E_{H_2O}. \quad (9)$$

Apart from the ion-dipole orientation of the probe water molecule plotted in Figure 2, three additional orientations with hydrogen atoms partially or completely pointing out to the actinide cation were included in the potential energy surface scan. The set of structures was fitted to the following site-site functional form which has been shown to behave properly in the description of the interaction of other highly charged metal cation hydrates with water molecules.[50,51,69] The addition of two extra terms ($r^{-4}$, $r^{-8}$) to the usual Lennard-Jones formulation allows more flexibility to describe the short- and medium-range interactions in the less attracting environment close to the aquaion as the intermediate regions,

$$E_{\mathrm{HIW}} = \sum_{i}^{\substack{\mathrm{HI}\\ \mathrm{sites}}} \sum_{j}^{\substack{\mathrm{Water}\\ \mathrm{sites}}} \left( \frac{C_4^{ij}}{r_{ij}^4} + \frac{C_6^{ij}}{r_{ij}^6} + \frac{C_8^{ij}}{r_{ij}^8} + \frac{C_{12}^{ij}}{r_{ij}^{12}} + \frac{q_i q_j}{r_{ij}} \right). \quad (10)$$

Fitting coefficients and RMSE are given in Table S4 of the supplementary material.

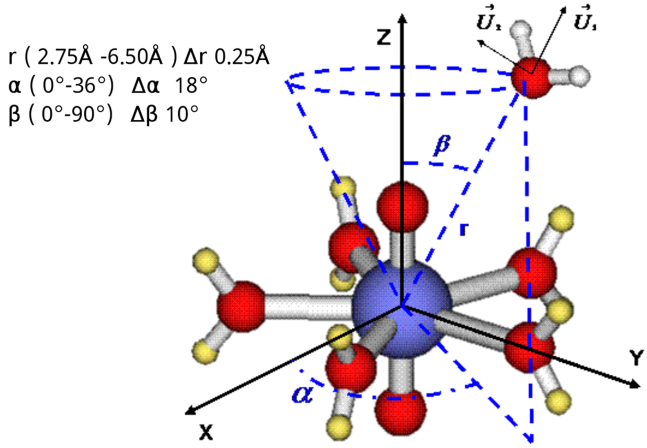


FIG. 2. Intermolecular geometrical parameters scanned in developing the HIW potential $[UO_2(H_2O)_5]^{2+}$–$H_2O$.

Once described the methodology proposed to build the set of intermolecular potentials of the uranyl cation in water, it is worth underlining the fact that the procedure is independent of the QM calculation level. This means that the choice of the computational level for a given molecular cation must be determined by the cost/accuracy ratio as a function of the physicochemical properties to be studied.

### B. Molecular dynamics simulations

MD simulations were run using the DL_POLY4 package.[70] The system was composed of one $[UO_2(H_2O)_5]^{2+}$ and 1495 TIP4P[71] $H_2O$ which corresponds to a concentration ~0.04 mol $kg^{-1}$. Simulations were run using a 14 Å cutoff for short-range interactions and particle mesh Ewald for the long-range Coulomb interactions. A 1 fs time step was used. The equations of motion were integrated using the velocity Verlet[72] and the NOSQUISH[73] quaternion algorithms. The system was initially minimized and then thermalized to 300 K for 0.5 ns with the Hoover thermostat. Then, a 0.5 ns NPT equilibration trajectory at 300 K and 1 bar was run using the Hoover barostat and thermostat with characteristic times of 0.5 ps on both. Finally, a 5 ns production run was performed. The final average density of the system was 1.001 g $cm^{-3}$.

## III. RESULTS AND DISCUSSION

### A. Hydration enthalpy

The hydration enthalpy ($\Delta H_{\mathrm{hyd}}$) of $[UO_2]^{2+}$ was computed according to

$$\Delta H_{\mathrm{hyd}} = H_{[UO_2]^{2+}(\mathrm{aq})} - H_{H_2O} - H_{[UO_2]^{2+}(\mathrm{g})}. \quad (11)$$

The different enthalpy values correspond to the average simulation enthalpy of: the aquaion in a box with 1495 water molecules, an equilibrated water box with the same total number of $H_2O$ molecules and $[UO_2]^{2+}$ in gas phase.

Our estimation of $\Delta H_{\mathrm{hyd}}(UO_2^{2+})$ is −333 ± 14 kcal $mol^{-1}$ which is within the range of experimental data. From the literature, an experimental $\Delta H_{\mathrm{hyd}}$ interval between −401 ± 15 kcal $mol^{-1}$ obtained by Gibson *et al.*[74] and −325 ± 5 kcal $mol^{-1}$ given by Marcus[75] is defined. The difficulties associated with the accurate quantification of gas phase formation enthalpy of actinides may be behind this substantial gap between experimental measurements.[76]

The TIP4P water model aside, we must point out that the $H_{[UO]_2^{2+}(\mathrm{aq})}$ estimation might be missing a small many-body contribution due to the first-second shell hydration.[49] Therefore, our $\Delta H_{\mathrm{hyd}}$ could be slightly overestimated, which suggested that our theoretical estimation is much closer to Marcus' value.

### B. Hydration structure of uranyl in aqueous solution

The uranium-oxygen RDF (Figure 3) shows three well defined peaks. The two first sharp peaks correspond to the two $O_{yl}$ and the five first shell oxygen atoms, $O_I$, at 1.76 Å and 2.46 Å, respectively. The third peak centered at 4.62 Å and extending up to ~6 Å corresponds to the second hydration shell.

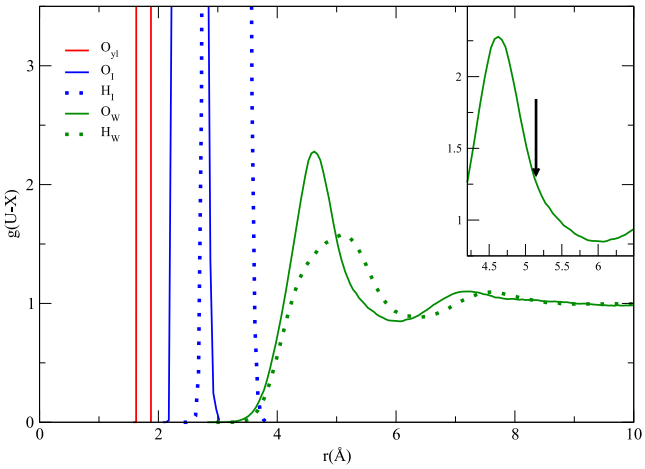


FIG. 3. U–O (solid lines) and U–H (dotted lines) radial distribution functions. Oxo oxygens (red), $O_{yl}$, first-shell $H_I$ and $O_I$ (blue) and second-shell $H_W$ and $O_W$ (green).

The main structural results in the literature and those of this study have been summarized in Table I. Our results are within the range of values for the U–$O_{yl}$, U–O, and U–H distances in the literature. In particular, they are quite similar to those reported by Bühl *et al.* from their CPMD simulation[77] and agree quite well with the experimental values reported from different techniques.[3,7,43,78]

The solvent effects on the $[UO_2(H_2O)_5]^{2+}$ induce opposite effects on the U–O bonds: the U–$O_{yl}$ bond-length is increased from 1.75 Å in gas phase to an average value of 1.76 Å in solution but the U–$O_I$ is shortened from 2.50 Å in the isolated cluster to 2.46 Å in solution. CPMD simulations[77] and QM studies[21,31] when a second hydration shell is added to the metal hydrate show the same effect.

The running coordination number (CN) of the second hydration shell obtained using the U–$O_W$ RDF (Figure 3) is 29. This striking value compelled us to revise the analysis. For most highly charged monatomic cations, it is a number slightly bigger than twice the CN of the first shell, because, on average, they can form two hydrogen bonds (HB) with two different second-shell water molecules and some additional packing water molecules.[32,44,51] However, we obtain three times this value. Due to the non-spherical symmetry of uranyl, one could wonder if the second peak in the RDF collects non-second-shell water molecules which artificially increase the CN.

The molecular axis formed by the U–$O_{yl}$ bonds and the perpendicular plane defined by the first-shell oxygen water molecules allow us to examine contributions to U−$O_w$ (and U−$H_w$) RDFs from different regions around the hydrated uranyl. Figure 4(b) plots the three selected regions: the equatorial one corresponds to the volume obtained by the rotation of the generatrix with azimuthal angles in the range 60°–90°; the axial region corresponds to the cone obtained when the azimuthal angle is 0°-30°, and the intermediate region corresponds to the volume obtained by the angles 30°-60°. A detailed description of this type of decomposition of the total RDF in angle-solved contributions can be found elsewhere.[82] Figure 4(a) plots the U−$O_w$ and U−$H_w$ angle-solved distribution functions. The maxima corresponding to the second-shell peak appear at 4.65 Å for the equatorial region, 4.35 Å for the intermediate region, and 4.85 Å for the axial region with integration numbers (for both hemispheres) of 10, 12, and 4, respectively. The relative position of the peak for the U−$H_w$ partial RDFs indicates that the water molecules in the equatorial region follow mainly an ion-dipole orientation since their tilt angle is close to 180°. This value is reduced in the intermediate region and the U−$H_w$ maximum appears at a shorter distance than the U−$O_w$ in the axial region. The peak minimum for the axial and intermediate regions appears at 6.0-6.4 Å which is about 1 Å higher than in the equatorial region (~5.3 Å). Thus, the second-shell minimum of the total RDF (~6.0 Å in Figure 3) encompasses not only the water molecules interacting with the first shell but additionally the $O_{yl}$ solvation. The equatorial RDF integrates to a number of $H_2O$ molecules which correspond to the typical hydration of monatomic cations. Furthermore, if we compute the average number of HB of the first-shell water molecules with second-shell water molecules (according to Chandler's definition[83]) we obtain 1.9 per water molecule, i.e., the classical cation hydration picture.

There is some discrepancy on the structure adopted by the solvent in the axial region. Wipff and Guilbaud[33,79] and Keristi and Liu[34] from MD using empirical interaction potentials, and Siboulet *et al.*[21] from QM computations found one hydrogen atom at around 1.8 Å from the uranyl oxygen forming typical hydrogen bonding. On the contrary, Roos *et al.*[35] and Maginn *et al.*[37,38] with classical MD using *ab initio* potentials;

TABLE I. Structural parameters corresponding to the hydration of $UO_2^{2+}\cdot n\ H_2O$ water derived from different experimental and theoretical sources. Distances are given in Å.

| Source | R(U–$O_{yl}$) | R(U–$O_I$) | $N_I$ | R(U–$O_{II}$) | $N_{II}$ | R(U–$H_I$) | R(U–$H_{II}$) | R($O_{yl}$–O) | R($O_{yl}$–H) |
|---|---|---|---|---|---|---|---|---|---|
| This work | 1.76 | 2.46 | 5[a] | 4.62 | 22[b] | 3.13 | 5.09 | 3.43 | 5.9 |
| CPMD[41,42,77] | 1.77-1.81 | 2.44-2.48 | 5 | 4.59-4.6 | 14-16 | | | | |
| *Ab initio* CMD[35,37,38] | 1.71-1.76 | 2.40-2.46 | 5 | 4.6-4.7 | 16-19 | | | 3.0 | 3.7 |
| Empirical CMD[33,34,79] | 1.80-1.89 | 2.40-2.5 | 5 | 4.3-4.7 | 15-19 | | 5.2[c] | 2.96-3.01 | 1.8-2.08 |
| QM gas phase clusters[21,80] | 1.77-1.79 | 2.42-2.43 | 5[a] | 4.5-4.6 | 10[a] | | | 1.8-1.92 | |
| High energy x-ray scattering[3,7] | 1.702-1.77 | 2.42 | 5[d] | 4.46 | 15 | | | | |
| EXAFS[43,78] | 1.76 | 2.41 | 5.2-5.3 | | | | | | |

[a]Fixed value.
[b]Using the multisite solute hydration number definition.[81]
[c]$N_{II}$ = 31-42.
[d]An equilibrium 88:12 five:four coordination is proposed.

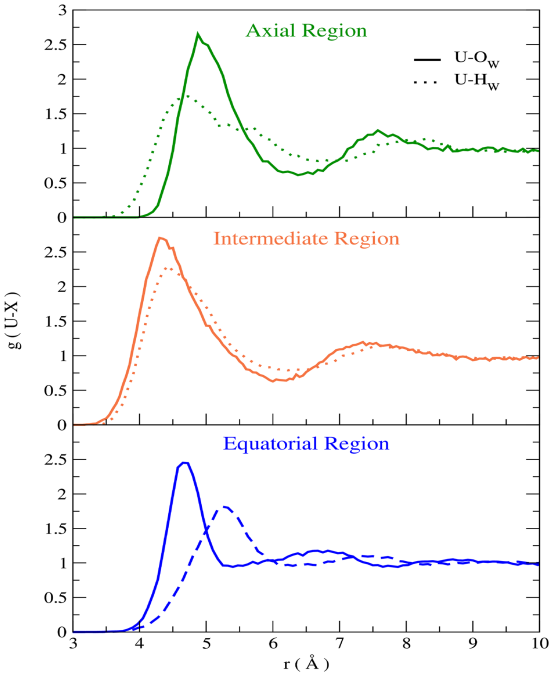


a)

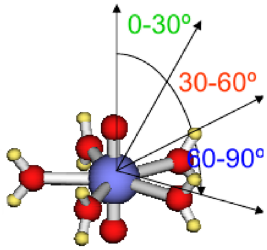


b)

FIG. 4. (a) shows the RDF for the axial region (0°-30°), the intermediate region (30°-60°), for the equatorial region (60°-90°). g(U−O$_w$) (solid lines) and g(U−H$_w$) (dotted lines). (b) defines the hydration angular regions.

Bühl *et al.*,[77] Frick *et al.*,[42] and Nichols *et al.*[41] using *ab initio* MD did not find preferential HB formation; furthermore, a low density number region is obtained, which led them to propose a rather *hydrophobic* behaviour in the uranyl axial region.

Our model clearly supports the non-hydrophilic structure of the axial region. In the 0°–90° O$_{yl}$ angle solved RDF (Figure 5(b)) the H and O first peak overlap. If the O$_{yl}$ atom had anionic character, the H maximum would be closer to the reference atom than the O maximum due to the formation of a H bond. The Spatial Distribution Function (SDF)[54] of the simulation is displayed in Figure 6. Water molecules occupy mainly the equatorial and intermediate regions, and the axial region is de-populated. Each axial region contains an average of 2.5 molecules at a distance of 3.35 Å. A snapshot of the simulation in Figure 7 depicts the hydration in that region. Axial water molecules H-bond preferentially among them than to the O$_{yl}$ atom, this reinforcement of the water structure is a typical characteristic of the hydrophobic hydration.[84,85] The SDF also shows that the hydration structure of $[UO_2(H_2O)_5]^{2+}$ resembles a sphere with the poles cut due to the lack of hydration of the O$_{yl}$ atoms.

The fact that the intermolecular potentials developed are based on the explicit QM assumption of a hydrated uranyl as the key species in solution allows a fine tuning of the interactions of the first and second hydration shell with the molecular cation and among them. This gives an even-tempered description of all the interactions in the close environment of the uranyl. As a result, it is found that the axial hydration mainly adopts a solvent structure, slightly perturbed by the presence of the uranyl oxygen and the cation charge, whereas in the equatorial region the strongly polarized uranyl-first shell water mediated an ordered second-shell structure in its environment.

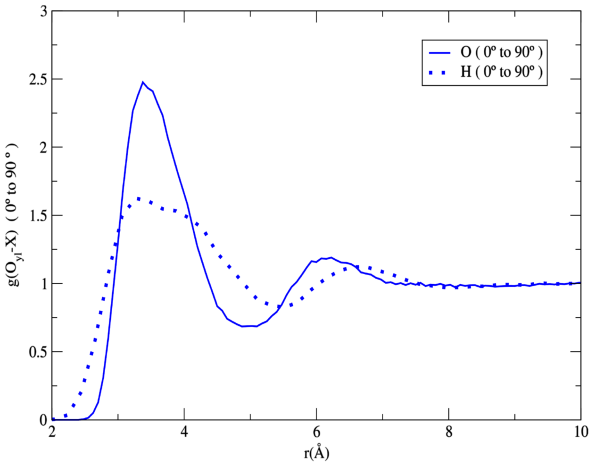


a)

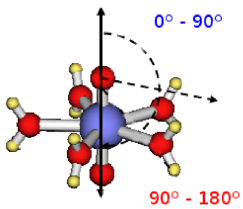


b)

FIG. 5. (b) shows the RDF for the 0°-90°. (a) defines the hydration angular regions. g(O$_{yl}$–O) (solid lines) and g(O$_{yl}$–H) (dotted lines).

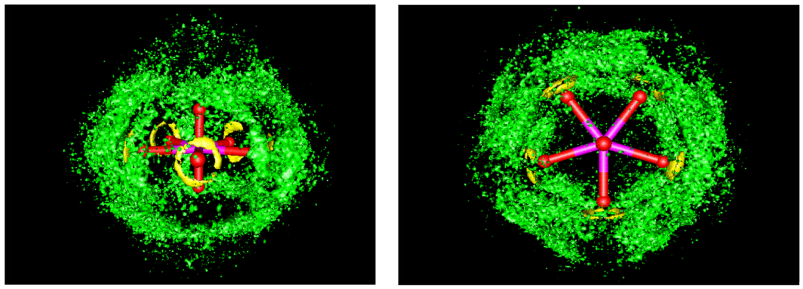

a) b)

FIG. 6. $[UO_2(H_2O)_5]^{2+}$(aq) spatial distribution function from the MD simulation: first shell H probability density (yellow) and bulk O water probability density (green). The isodensity surfaces contain 20% of the total probability.

The CNs of the second shell obtained with high energy x-ray scattering and most MD simulations are quite smaller than the value obtained from the total U–$O_W$ RDF integration. Nevertheless, this high value is a direct consequence of using a radial distribution function that is spherically averaged to measure coordination in non-spherically symmetric environments. Our RDFs are complex, for example, having an inflection point at ~5 Å in the U–$O_W$ RDF (see inset in Figure 3). Its integration assigns bridge water molecules to the coordination of $O_{yl}$ and $O_I$ artificially. The computation of the solute CN based on the multisite cavity definition developed by our group for asymmetric coordination environments avoids this artifact.[81] This CN is defined as the average number of water molecules within the cavity formed by the overlapping of spheres centered on solvent exposed atoms ($O_I$ and $O_{yl}$, in our case), whose radii correspond to the minima of angle-solved X–$O_W$ RDFs. Employing this definition, we obtain a second coordination shell value of 22 which is closer to the range of literature values and is consistent with our angle-solved analysis. In order to test this multisite cavity method and the intermolecular potentials developed, a similar MD simulation to the one presented here was carried out using the potential of Maginn *et al.*[37] The multisite-cavity CN was in this case 20, and the cavity volume was 730 Å$^3$, whereas our cavity had a volume of 697 Å$^3$. Figure 8 shows the solute multisite-cavity that encloses the water molecules counted to obtain the CNs. Finally, the second-shell CN in high energy x-ray scattering experiment can only be considered a lower bound of the value for a dilute solution because the samples have an $UO_2(ClO_4)_2$ concentration of 0.5 mol kg$^{-1}$.

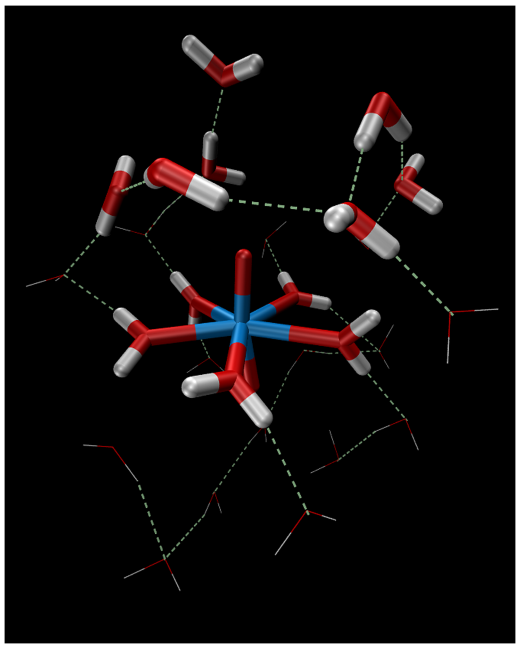

FIG. 7. $[UO_2(H_2O)_5]^{2+}$ MD snapshot showing only some water molecules with an axial view and HB according to Chandler's definition.[83]

### C. Water mean residence time

In Table II we present the mean residence time (MRT) of solvent molecules in the second shell computed by the method of Impey *et al.*[86] The MRT of a water molecule in the first shell of another water molecule in a TIP4P water simulation is included for comparison. We allow two possible time intervals ($t^*$) for the water molecule to leave the shell and return still ascribing it to the shell, $t^*_{2ndshell} = 0$ ps and $t^*_{2ndshell} = 2$ ps. These values are generally accepted to provide a good range in the literature.[86,87] We have also studied the residence times in the regions defined by the angle-solved distribution functions defined in Figure 5.

The total MRT of a water molecule in the $[UO_2]^{2+}$ second shell has a value of 8 and 17 ps for $t^*_{2ndshell} = 0$ ps and $t^*_{2nd} = 2$ ps, respectively. The MRT is much higher than the 0.4 ps and 5.6 ps obtained in QMCF *ab initio* MD by Frick *et al.*[42] Additionally, our value is greater than that for other divalent cation aqueous solutions like that of $Mg^{2+}$ having values of 3 ps and 14 ps.[51] This is likely due to the much higher volume of the second hydration shell of a molecular cation, such as $[UO_2]^{2+}$. The comparison of the angle-solved and the total MRT shows that

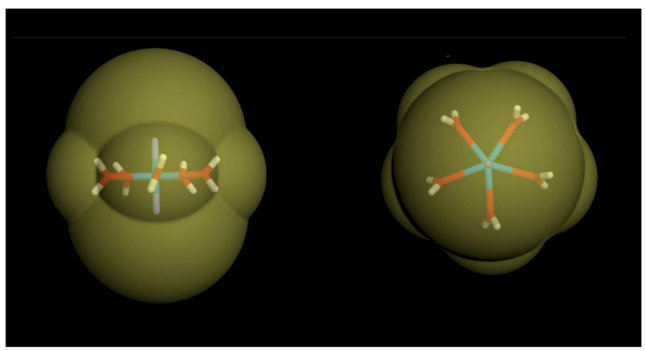

FIG. 8. Multisite solute cavity for the hydrated ion model of $[UO_2(H_2O)_5]^{2+}$ with a volume of 697 Å$^3$.

TABLE II. Mean residence times (ps) of $H_2O$ in the second shell of $[UO_2]^{2+}$ with maximum transient period out of the shell $t^* = 0$ ps and $t^* = 2$ ps and its decomposition in the angular regions of Figure 4(a). For comparison the MRT of TIP4P water in the first shell of another water molecule in a pure water simulation is included.

| Region | $t^*_{2ndshell} = 0$ ps | $t^*_{2ndshell} = 2$ ps |
|---|---|---|
| Total MRT (2nd shell) | 8 ± 1 | 17 ± 1 |
| 0°-30° (2nd shell) | 1 ± 1 | 6 ± 1 |
| 30°-60° (2nd shell) | 1 ± 1 | 8 ± 1 |
| 60°-90° (2nd shell) | 2 ± 1 | 10 ± 1 |
| $H_2O$ (1st shell) | 1.39 ± 0.02 | 4.19 ± 0.06 |

the equatorial second shell has lower exchange rates with bulk solvent molecules than the axial second shell. Solvent motion within the different angular regions of the second shell explains the difference between total and partial MRTs.

The solvent MRT in the axial regions is higher than in the first-shell of a bulk water molecule. This indicates that the water-water interactions around the hydrophobic $O_{yl}$ region are reinforced with respect to solution. The enhancement of the water structure around a hydrophobic solute is a dynamical characteristic of a clathrate-like hydration.[84,85]

### D. Self-diffusion coefficient

The self-diffusion coefficient, $D_0$, for the $[UO_2(H_2O)_5]^{2+}$ in the MD simulation was computed using the Einstein formula. An initial value of $(0.8 \pm 0.1)\ 10^{-5}$ cm$^2$ s$^{-1}$ was obtained. Due to the use of periodic boundary conditions, diffusion coefficients from MD simulations are always underestimated. The neighboring images of each atom couple viscously reducing their motion and reducing $D_0$. This effect can be corrected for a cubic cell using the Yeh and Hummer expression,[88]

$$D_0^{\text{corr}} = D_0 + \frac{k_B T \xi}{6\pi\eta L}, \tag{12}$$

where $\eta$ is the solvent viscosity, $L$ the average simulation box size, and $\xi$ the so called self-term which for a cubic lattice at room temperature is 2.837 298. Using the TIP4P water viscosity at 300 K, a $D_0^{\text{corr}} = (1.1 \pm 0.1)\ 10^{-5}$ cm$^2$ s$^{-1}$ value is obtained. The experimental self-diffusion coefficient for $[UO_2]^{2+}$ at infinite dilution is $(0.67 \pm 0.01)\ 10^{-5}$ cm$^2$ s$^{-1}$.[89,90] The simulated value only has the right order of magnitude of the experimental. The TIP4P water model overestimates the self-diffusion coefficient of water by ~50%; therefore since the water molecules around the cation move too fast, the cation is more free to move than if the water dynamics was more accurate. A usual correction, employed by several authors,[34,46,91] is the normalization of the obtained diffusion coefficient by the pure water model diffusion coefficient, in our case $D_0^{\text{corr}}/D_0^{\text{TIP4P}} = 0.4 \pm 0.1$. This value is close to the normalized experimental diffusion coefficient, $D_0^{\text{exp}}/D_0^{\text{wat}} = 0.3 \pm 0.01$, revealing that our $[UO_2]^{2+}$ dynamics is partly biased by the water model diffusion.

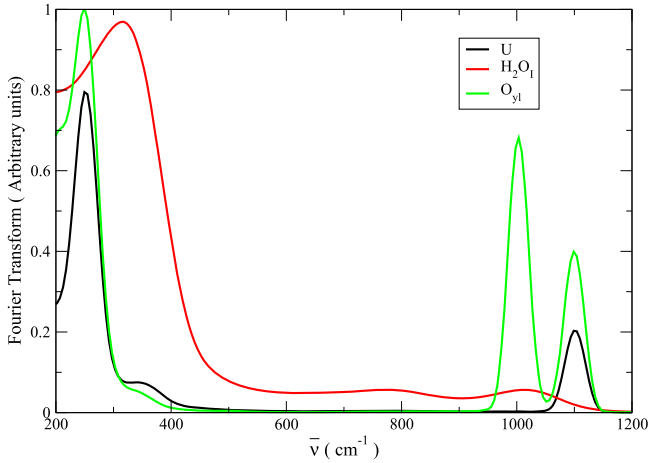


FIG. 9. Power spectra of the velocity autocorrelation function of the U, $O_{yl}$, and $H_2O_I$ atom types of the MD simulation.

### E. Power spectra

The power spectra of the velocity autocorrelation (VAC) functions of the atoms of $[UO_2(H_2O)_5]^{2+}$ from the simulation trajectory have been computed and plotted in Figure 9. To make easier the assignment of the bands, internal coordinates associated with a particular normal mode have been defined.[51,92] For the $[UO_2]^{2+}$ bending motion, with irreducible representation $E_1$, $\phi$ was defined as the $O_{yl}$–U–$O_{yl}$ angle and its cosine function used to compute its autocorrelation function,

$$\left\langle \left(\cos(\phi) - \overline{\cos(\phi)}\right) \cdot \left(\cos(\phi) - \overline{\cos(\phi)}\right) \right\rangle. \tag{13}$$

The Fourier transform of the autocorrelation function is performed to obtain the normal mode frequencies. The rest of the internal coordinates for the symmetric ($1A_1$) and antisymmetric ($A_2$) U–$O_{yl}$ stretching as well as the water breathing symmetric U–$O_I$ stretching ($2A_1$) are defined in the supplementary material. Table III presents the frequencies obtained with several simulation conditions and models, together with experimental data.

TABLE III. Normal mode frequencies, $\bar{\nu}$ (cm$^{-1}$) for $[UO_2(H_2O)_5]^{2+}$ with different models and experiment. The uncertainties in our theoretical results are ±5 cm$^{-1}$.

| System | Method | $E_1$ | $2A_1$ | $1A_1$ | $A_2$ |
|---|---|---|---|---|---|
| $[UO_2(H_2O)_5]^{2+}$(g) | B3LYP | 224 | 314 | 945 | 1028 |
| $[UO_2(H_2O)_5]^{2+}$(g) | MD 5 K | 181 | 298 | 982 | 1080 |
| $[UO_2(H_2O)_5]^{2+}$(g) | MD 300 K | 256 | 286 | 977 | 1027 |
| $[UO_2(H_2O)_5]^{2+}$(aq) | MD 300 K, 1 bar | 252 | 338 | 1004 | 1101 |
| $[UO_2(H_2O)_5]^{2+}$(aq) | Experimental | 253 ± 10[93] | | 874 ± 10[93,94] | 965 ± 10[94] |

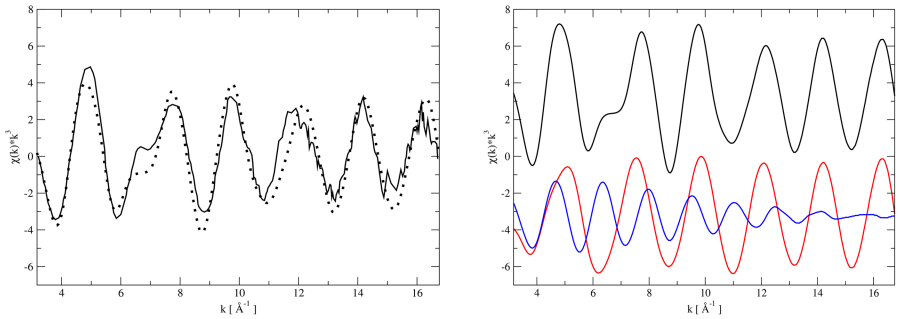


FIG. 10. $[UO_2(H_2O)_5]^{2+}L_{III}$-edge $k^3$-weighted EXAFS spectra. (a) Experimental[43] 0.01M $[UO_2]^{2+}$, 0.1M $HClO_4$ EXAFS data (solid line), and simulated spectrum (dotted line). (b) Simulated spectrum (black), $O_{yl}$ path (red line) contributions to the simulated spectrum, and $O_I$ path contributions (blue line) to the simulated spectrum.

The normal mode frequencies obtained in solution are close to the experimental ones, with a maximum 15% error for the $1A_1$. The fact that the stretching modes are overestimated is due in part to the B3LYP potential energy surface that biases our frequencies in that sense, particularly for $1A_1$ and $A_2$, and to the performance of the intermolecular potentials developed.

The normal mode frequencies are a measure of the fit of the classical potential to the QM potential energy surface. It is worth pointing out that the interaction potential contains no harmonic terms, unlike the majority of force fields. Therefore, simulation frequencies contain all the anharmonicities that the surface presents since, unlike static standard QM methods, no harmonic model is assumed.

Bearing in mind these facts, the comparison of the $[UO_2(H_2O)_5]^{2+}$ frequencies in gas phase using the B3LYP harmonic normal modes and those obtained from low temperature MD simulation (Table III) supports the good potential performance. Gas phase room temperature MD simulation frequencies shift with respect to their low temperature counterparts. This shifting is partly due to the anharmonicities of the potential energy surface explored at higher temperatures and to the coupling of the modes to the bulk water motion. Running the high temperature simulation with the water molecules frozen yields frequencies (not shown) nearly identical to those at low temperature, therefore, the coupling of the first shell water motions to the molecular cation normal modes is the main responsibility of the shifts.

The $[UO_2(H_2O)_5]^{2+}$ frequencies obtained from MD simulations at 300 K in solution and in the gas phase have only small change for the modes involving uranyl, which reflects the small perturbation induced by solvation on the $[UO_2]^{2+}$ entity. Contrarily, the U–$O_I$ stretching is more affected in relative terms due to the second shell effects.

### F. EXAFS spectrum simulation

X-ray absorption spectroscopy is a powerful technique to obtain accurate short range structural information around a metal ion in solution.[95,96] The comparison between the experimental EXAFS spectrum of a given sample and the simulated one derived from a set of configurations extracted from a statistical computer simulation has become a useful tool for intramolecular potential assessment.[52,97,98] The simulated EXAFS spectrum for uranyl in water has been computed as the average of the individual spectra of 200 configurations of $[UO_2]^{2+}$ including its two first coordination shells from the MD trajectory using the FEFF 9.0 code.[99] The average $L_{III}$-edge $k^3$-weighted spectrum including multiple scattering up to four-legged paths was computed. Figure 10 compares the simulated spectrum with the experimental spectrum of a 0.01M $[UO_2]^{2+}$(aq) solution in 0.1 M perchloric acid.[43] Details of the method to simulate the EXAFS spectrum can be found elsewhere.[52,69] The similarity between the main features of the simulated and experimental spectra validates our atomistic representation of the uranyl aqueous solution. The calculated spectra reproduce satisfactorily the experimental frequency, and slightly underestimate the signal decay. The spectrum is unchanged if only the first hydration shell is included in the calculations. This means that the second shell cannot be detected by EXAFS for this system.

We obtain Debye-Waller factors of $6.5 \cdot 10^{-4}$ Å$^2$ and $6.8 \cdot 10^{-3}$ Å$^2$ for U–$O_{yl}$ and U–$O_W$, respectively, which are close to the experimental values[43] of $1.6 \cdot 10^{-3}$ Å$^2$ and $7.1 \cdot 10^{-3}$ Å$^2$.

The shoulder at ~6.5 Å$^{-1}$ has a lower intensity in the simulated spectrum than in the experimental. To study this, we decomposed this complex spectrum into its U–$O_{yl}$ and U–$O_I$ contributions (together with multiple scattering paths where $O_{yl}$ and $O_I$ backscatters are included) in Figure 10. Both contributions are produced mainly by the single-scattering paths. The U–$O_{yl}$ paths (red line) have a slow decay and high intensity due to the small disorder associated with the strong covalent bonds U–$O_{yl}$. In contrast, contributions due to the $O_I$ involved paths (blue line) generate a weaker signal with a damped oscillation which decays faster than its counterpart. The frequency of the latter contribution is higher since the U–$O_I$ distance is larger than that of the U–$O_{yl}$ bond. The shoulder is a feature produced by the superposition of single scattering paths and not a multiple scattering phenomenon that other structures with planar backscattering configurations present.

## IV. CONCLUDING REMARKS

We have extended the hydrated ion model for the development of intermolecular potentials to the case of molecular metal cation, including its flexibility. The set of intermolecular potentials represents correctly the model potential energy surface and the properties derived from the analysis of the MD trajectory are in agreement with experimental data. It is worth mentioning that the broad scope of spectroscopic, energetic, dynamical, and structural properties are well described. The second-shell CNs obtained from RDFs are overestimated since they count bridge water molecules and even third-shell

water molecules as the angle-solved RDFs have shown. Using the definition of a multisite cavity for the solute to compute the CN, the overestimated value is eliminated obtaining a CN closer to previously published results. These RDFs also show a very weak solvation of the $O_{yl}$ atoms implying a hydrophobic behavior without preferential H bond formation with the solute, but reinforcement of the water network. This fact, in addition to the reinforcement of the axial water structure shown by the MRT, gives evidence of clathrate-like solvation around the $O_{yl}$ atoms. Their weak solvation is also manifested by the absence of frequency shifts in the uranyl stretching and bending normal modes of the pentahydrate isolated or in solution. In contrast, the equatorial solvation structure resembles that of monatomic divalent cations. The hydration structure of the $[UO_2]^{2+}$ cation is striking since its hydrophilic and hydrophobic regions are very close together on a small solute in contrast to most amphiphilic solutes. The intermediate hydration region contains a set of water molecules which fit both regions smoothly. The hydration structure of $[UO_2]^{2+}$ is strongly anisotropical, being the result of coupling a conventional hydration sphere in the equatorial region with clathrate-like caps, mediated by bridge water molecules in the intermediate region. Based on previous experience with the hydrated ion model,[51] the generalization of the set of intermolecular potentials for $[UO_2]^{2+}$ in water could be easily extended to the series of actinyls, $[AnO_2]^{q+}$. Therefore, the set of new potentials presented here will be the starting point for the description of other actinyls in solution or confined condensed media, e.g., layered silicates.

## SUPPLEMENTARY MATERIAL

See supplementary material for the atomic partial charges and Merz-Kollman radii; deformations of the pentahydrate to fit the force field; interaction potential coefficients and quality of fit parameters; and normal mode internal coordinate definition.

## ACKNOWLEDGMENTS

This work was financially supported by Junta de Andalucía of Spain (Proyecto de Excelencia, No. P11-FQM 7607) and the Spanish Ministry of Education, Culture and Sports for the Ph.D. scholarship FPU (Formación de Profesorado Universitario) awarded to SPC.

[1] S. Cotton, *Lanthanide and Actinide Chemistry* (Wiley, London, 2006).
[2] N. Bardin, P. Rubini, and C. Madic, Radiochim. Acta **83**, 189 (1998).
[3] M. Åberg, D. Ferri, J. Glaser, and I. Grenthe, Inorg. Chem. **22**, 3986 (1983).
[4] W. D. Loveland, D. J. Morrissey, and G. T. Seaborg, *Modern Nuclear Chemistry* (John Wiley & Sons, 2006).
[5] S. D. Conradson, Appl. Spectrosc. **52**, 252 (1998).
[6] U. Wahlgren, H. Moll, I. Grenthe, B. Schimmelpfennig, L. Maron, V. Vallet, and O. Gropen, J. Phys. Chem. A **103**, 8257 (1999).
[7] J. Neuefeind, L. Soderholm, and S. Skanthakumar, J. Phys. Chem. A **108**, 2733 (2004).
[8] K. L. Nash and G. J. Lumetta, *Advanced Separation Techniques for Nuclear Fuel Reprocessing and Radioactive Waste Treatment* (Woodhead, 2011).
[9] J. M. McKibben, Radiochim. Acta **36**, 3 (1984).
[10] M. Dolg, *Lanthanides and Actinides* (John Wiley, Chichester, 1999), p. 1478.
[11] L. Seijo, Z. Barandiaran, and E. Harguindey, J. Chem. Phys. **114**, 118 (2001).
[12] P. J. Hay and R. L. Martin, J. Chem. Phys. **109**, 3875 (1998).
[13] P. A. Malmqvist, B. O. Roos, and B. Schimmelpfennig, Chem. Phys. Lett. **357**, 230 (2002).
[14] V. Vallet, L. Maron, C. Teichteil, and J.-P. Flament, J. Chem. Phys. **113**, 1391 (2000).
[15] N. Kaltsoyannis, P. J. May, J. Li, J. P. Blaudeau, and B. E. Bursten, *The Chemistry of Actinide and Transactinide Elements*, 3rd ed. (Springer, Dordrecht, 2006), Chap. 17, p. 1893.
[16] L. Gagliardi and B. Roos, Nature **433**, 848 (2005).
[17] V. Vallet, P. Macak, U. Wahlgren, and I. Grenthe, Theor. Chem. Acc. **115**, 145 (2006).
[18] S. Tsushima and A. Suzuki, J. Mol. Struct.: THEOCHEM **487**, 33 (1999).
[19] S. Tsushima and A. Suzuki, J. Mol. Struct.: THEOCHEM **529**, 21 (2000).
[20] J. P. Blaudeau, S. A. Zygmunt, L. A. Curtiss, D. T. Reed, and B. E. Bursten, Chem. Phys. Lett. **310**, 347 (1999).
[21] B. Siboulet, C. Marsden, and P. Vitorge, Chem. Phys. **326**, 289 (2006).
[22] K. Ingram, L. Jonas, L. Häller, and N. Kaltsoyannis, Dalton Trans. 2403 (2006).
[23] S. Spencer, L. Gagliardi, N. C. Handy, A. G. Ioannou, and A. Simper, J. Phys. Chem. A **103**, 1831 (1999).
[24] P. J. Hay, R. L. Martin, and G. Schreckenbach, J. Phys. Chem. A **104**, 6259 (2000).
[25] S. Tsushima, T. Yang, and A. Suzuki, Chem. Phys. Lett. **334**, 365 (2001).
[26] L. V. Moskaleva, S. Krüger, A. Spörl, and N. Rösch, Inorg. Chem. **43**, 4080 (2004).
[27] Z. Cao and K. Balasubramanian, J. Chem. Phys. **123**, 114309 (2005).
[28] M. S. K. Fuchs, A. M. Shor, and N. Rösch, Int. J. Quantum Chem. **86**, 487 (2002).
[29] G. Shamov and G. Schreckenbach, J. Phys. Chem. A **109**, 10961 (2005).
[30] E. Sánchez Marcos, R. R. Pappalardo, and D. Rinaldi, J. Phys. Chem. **95**, 8928 (1991).
[31] J. M. Martínez, R. R. Pappalardo, and E. Sánchez Marcos, J. Phys. Chem. A **101**, 4444 (1997).
[32] Y. Marcus, *Ions in Solution and Their Solvation*, 1st ed. (John Wiley & Sons, 2015).
[33] P. Guilbaud and G. Wipff, J. Phys. Chem. **97**, 5685 (1993).
[34] S. Kerisit and C. Liu, J. Phys. Chem. A **117**, 6421 (2013).
[35] D. Hagberg, G. Karlström, B. O. Roos, and L. Gagliardi, J. Am. Chem. Soc. **127**, 14250 (2005).
[36] A. Wallqvist, P. Ahlström, and G. Karlström, J. Phys. Chem. **94**, 1649 (1990).
[37] N. Rai, S. P. Tiwari, and E. J. Maginn, J. Phys. Chem. B **116**, 10885 (2012).
[38] V. Pomogaev, S. P. Tiwari, N. Rai, G. S. Goff, W. Runde, W. F. Schneider, and E. J. Maginn, Phys. Chem. Chem. Phys. **15**, 15954 (2013).
[39] M. Bühl, R. Diss, and G. Wipff, J. Am. Chem. Soc. **127**, 13506 (2005).
[40] R. Car and M. Parrinello, Phys. Rev. Lett. **55**, 2471 (1985).
[41] P. Nichols, E. J. Bylaska, G. K. Schenter, and W. de Jong, J. Chem. Phys. **128**, 124507 (2008).
[42] R. J. Frick, T. S. Hofer, A. B. Pribil, B. R. Randolf, and B. M. Rode, J. Phys. Chem. A **113**, 12496 (2009).
[43] C. Hennig, K. Schmeide, V. Brendler, H. Moll, S. Tsushima, and A. C. Scheinost, Inorg. Chem. **46**, 5882 (2007).
[44] D. T. Richens, *The Chemistry of Aqua Ions* (John Wiley, West Sussex, England, 1997).
[45] L. Helm and A. E. Merbach, Chem. Rev. **105**, 1923 (2005).
[46] S. P. Tiwari, N. Rai, and E. J. Maginn, Phys. Chem. Chem. Phys. **16**, 8060 (2014).
[47] E. Sánchez Marcos, R. R. Pappalardo, J. C. Barthelat, and F. Xavier Gadea, J. Phys. Chem. **96**, 516 (1992).
[48] R. R. Pappalardo and E. Sánchez Marcos, J. Phys. Chem. **97**, 4500 (1993).
[49] R. R. Pappalardo, J. M. Martínez, and E. Sánchez Marcos, J. Phys. Chem. **100**, 11748 (1996).
[50] J. M. Martínez, R. R. Pappalardo, and E. Sánchez Marcos, J. Chem. Phys. **109**, 1445 (1998).
[51] J. M. Martínez, R. R. Pappalardo, and E. Sánchez Marcos, J. Am. Chem. Soc. **121**, 3175 (1999).
[52] P. J. Merkling, A. Muñoz-Páez, and E. Sánchez Marcos, J. Am. Chem. Soc. **124**, 10911 (2002).
[53] E. Galbis, J. Hernández-Cobos, C. den Auwer, C. Le Naour, D. Guillaumont, E. Simoni, R. R. Pappalardo, and E. Sánchez Marcos, Angew. Chem. **122**, 3899 (2010).
[54] J. M. Martínez, F. Torrico, R. R. Pappalardo, and E. Sánchez Marcos, J. Phys. Chem. B **108**, 15851 (2004).
[55] F. Torrico, R. R. Pappalardo, E. Sánchez Marcos, and J. M. Martínez, Theor. Chem. Acc. **115**, 196 (2006).

[56]J. M. Martínez, R. R. Pappalardo, E. Sánchez Marcos, K. Refson, S. Díaz-Moreno, and A. Muñoz-Páez, J. Phys. Chem. B **102**, 3272 (1998).
[57]A. D. Becke, J. Chem. Phys. **98**, 5648 (1993).
[58]P. J. Stephens, F. J. Devlin, C. F. Chabalowski, and M. J. Frisch, J. Phys. Chem. **98**, 11623 (1994).
[59]W. Küchle, M. Dolg, H. Stoll, and J. Preuss, J. Chem. Phys. **100**, 7535 (1994).
[60]D. E. Woon and T. H. Dunning, Jr., J. Chem. Phys. **98**, 1358 (1993).
[61]M. J. Frisch, G. W. Trucks, H. B. Schlegel, G. E. Scuseria, M. A. Robb, J. R. Cheeseman, G. Scalmani, V. Barone, B. Mennucci, G. A. Petersson, H. Nakatsuji, M. Caricato, X. Li, H. P. Hratchian, A. F. Izmaylov, J. Bloino, G. Zheng, J. L. Sonnenberg, M. Hada, M. Ehara, K. Toyota, R. Fukuda, J. Hasegawa, M. Ishida, T. Nakajima, Y. Honda, O. Kitao, H. Nakai, T. Vreven, J. A. Montgomery, Jr., J. E. Peralta, F. Ogliaro, M. Bearpark, J. J. Heyd, E. Brothers, K. N. Kudin, V. N. Staroverov, R. Kobayashi, J. Normand, K. Raghavachari, A. Rendell, J. C. Burant, S. S. Iyengar, J. Tomasi, M. Cossi, N. Rega, J. M. Millam, M. Klene, J. E. Knox, J. B. Cross, V. Bakken, C. Adamo, J. Jaramillo, R. Gomperts, R. E. Stratmann, O. Yazyev, A. J. Austin, R. Cammi, C. Pomelli, J. W. Ochterski, R. L. Martin, K. Morokuma, V. G. Zakrzewski, G. A. Voth, P. Salvador, J. J. Dannenberg, S. Dapprich, A. D. Daniels, Ö. Farkas, J. B. Foresman, J. V. Ortiz, J. Cioslowski, and D. J. Fox, GAUSSIAN 09, Revision D.01, Gaussian, Inc., Wallingford, CT, 2009.
[62]L. Soderholm, S. Skanthakumar, and J. Neuefeind, Anal. Bioanal. Chem. **383**, 48 (2005).
[63]L. Sémon, C. Boeheme, I. Billard, C. Hennig, K. Lüzenkirchen, T. Reich, A. Roßberg, I. Rossini, and G. Wipff, ChemPhysChem **2**, 591 (2001).
[64]U. C. Singh and P. A. Kollman, J. Comput. Chem. **5**, 129 (1984).
[65]B. H. Besler, K. M. Merz, and P. A. Kollman, J. Comput. Chem. **11**, 431 (1990).
[66]S. Miertus, E. Scrocco, and J. Tomasi, Chem. Phys. **55**, 117 (1981).
[67]B. Mennucci, E. Cancès, and J. Tomasi, J. Phys. Chem. B **101**, 10506 (1997).
[68]S. Batsanov, Inorg. Mat. **37**, 871 (2001).
[69]F. Carrera, F. Torrico, D. T. Richens, A. Muñoz-Páez, J. M. Martínez, R. R. Pappalardo, and E. Sánchez Marcos, J. Phys. Chem. B **111**, 8223 (2007).
[70]I. T. Todorov, W. Smith, K. Trachenko, and M. T. Dove, J. Mater. Chem. **16**, 1911 (2006).
[71]W. L. Jorgensen, J. Chandrasekhar, J. D. Madura, R. W. Impey, and M. L. Klein, J. Chem. Phys. **79**, 926 (1983).
[72]W. C. Swope, H. C. Andersen, P. H. Berens, and K. R. Wilson, J. Chem. Phys. **76**, 637 (1982).
[73]T. Miller, M. Eleftheriou, P. Pattnaik, A. Ndirango, D. Newns, and G. Martyna, J. Chem. Phys. **116**, 8649 (2002).
[74]J. K. Gibson, R. G. Haire, M. Santos, J. Maralo, and A. Pires de Matos, J. Phys. Chem. A **109**, 2768 (2005).
[75]Y. Marcus and A. Loewenschuss, J. Chem. Soc., Faraday Trans. 1 **82**, 2873 (1986).
[76]L. V. Moskaleva, A. V. Matveev, S. Krüger, and N. Rösch, Chem. - Eur. J. **12**, 629 (2006).
[77]M. Bühl, H. Kabrede, R. Diis, and G. Wipff, J. Am. Chem. Soc. **128**, 6357 (2006).
[78]P. Allen, J. Bucher, D. Shuh, N. Edelstein, and T. Reich, Inorg. Chem. **36**, 4676 (1997).
[79]P. Guilbaud and G. Wipff, J. Mol. Struct.: THEOCHEM **366**, 55 (1996).
[80]K. E. Gutowski and D. A. Dixon, J. Phys. Chem. A **110**, 8840 (2006).
[81]A. Melchior, J. M. Martínez, R. R. Pappalardo, and E. Sánchez Marcos, J. Chem. Theory Comput. **9**, 4562 (2013).
[82]E. C. Beret, J. M. Martínez, R. R. Pappalardo, E. Sánchez Marcos, N. L. Doltsinis, and D. Marx, J. Chem. Theory Comput. **4**, 2108 (2008).
[83]A. Luzar and D. Chandler, Phys. Rev. Lett. **76**, 928 (1996).
[84]P. Ball, Chem. Rev. **108**, 74 (2008).
[85]E. I. Martín, J. M. Martínez, and E. Sánchez Marcos, J. Chem. Phys. **143**, 044502 (2015).
[86]R. Impey, P. Madden, and I. McDonald, J. Phys. Chem. **87**, 5071 (1983).
[87]A. E. García and L. Stiller, J. Comput. Chem. **14**, 1396 (1993).
[88]I.-C. Yeh and G. Hummer, J. Phys. Chem. B **108**, 15873 (2004).
[89]J.-P. Simonin, I. Billard, H. Hendrawan, O. Bernard, K. Lützenkirchen, and L. Sémon, Phys. Chem. Chem. Phys. **5**, 520 (2003).
[90]D. Kern and E. Orlemann, J. Am. Chem. Soc. **71**, 2102 (1949).
[91]M. Chopra and N. Choudhury, J. Phys. Chem. B **118**, 14373 (2014).
[92]R. J. H. Clark and R. E. Hester, *Advances in Infrared and Raman Spectroscopy* (Hayden, 1983), Chap. 6.
[93]M. Gál, P. Goggin, and J. Mink, Spectrochim. Acta, Part A **48**, 121 (1992).
[94]C. Tait, in Symposium of Heavy Element Complexes, 217th ACS National Meeting, Anaheim, CA, 1999.
[95]D. Koningsberger and R. Prins, *X-Ray Absorption: Principles, Applications, Techniques of EXAFS, SEXAFS, and XANES* (John Wiley and Sons, New York, NY, 1988).
[96]M. A. Denecke, Coord. Chem. Rev. **250**, 730 (2006).
[97]A. Filipponi, P. D'Angelo, N. V. Pavel, and A. Di Cicco, Chem. Phys. Lett. **225**, 150 (1994).
[98]B. J. Palmer, D. M. Pfund, and J. L. Fulton, J. Phys. Chem. **100**, 13393 (1996).
[99]A. L. Ankudinov, A. I. Nesvizhskii, and J. J. Rehr, Phys. Rev. B **67**, 115120 (2003).